THE JOURNAL OF PHYSICAL CHEMISTRY C
A JOURNAL OF THE AMERICAN CHEMICAL SOCIETY

pubs.acs.org/JPCC

Article

Simulation of STM Images of Hematite α-Fe_2O_3(0001) Surfaces: Dependence on Distance and Bias

Tomasz Ossowski, Tomasz Pabisiak, Adam Kiejna,* Krisztián Palotás, and Ernst Bauer

Cite This: *J. Phys. Chem. C* 2021, 125, 26711−26717

Read Online

ACCESS | Metrics & More | Article Recommendations | Supporting Information

ABSTRACT: Experimental scanning tunneling microscopy (STM) images of the hematite (0001) surface exhibit long-range superstructures formed by coexisting domains consisting of different terminations (α, β, γ) of the α-Fe_2O_3(0001) surface. In this work extensive simulations of STM images of different terminations of hematite (0001) surfaces are performed and compared with measured ones in order to identify the nature of the superstructure unit meshes. Based on DFT calculations of α-Fe_2O_3(0001) surfaces, the STM images are simulated using Chen's derivative rules approach. Different bias voltages and tip−sample distances as well as the role of the tip type are considered and discussed. For some terminations an extreme dependence of the simulated image on the distance and bias voltage is found. The difference between simulations of metal and insulator/semiconductor surfaces is discussed. The condition of simultaneous agreement between simulation and experiment for all terminations within a narrow STM parameter range leads to the assignment of the α, β and γ terminations to the ferryl, Fe-Fe−O_3− or Fe−O_3−Fe−, and O_3−Fe−Fe− terminations, respectively.

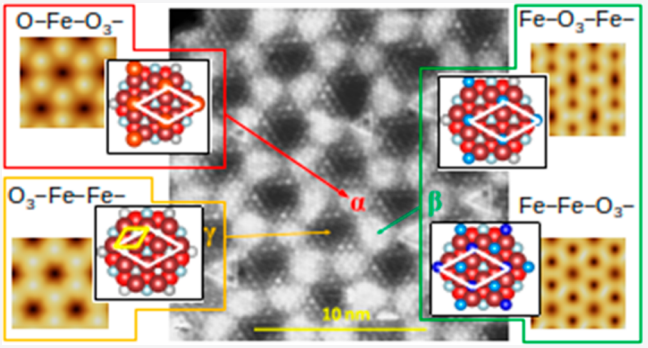

INTRODUCTION

Iron oxides are of great importance in physics, chemistry, and different technologies ranging from spintronics to heterogeneous catalysis. They occur in nature in various structures and compositions.[1] The best known and most studied iron oxide is hematite (α-Fe_2O_3) crystallizing in the corundum structure. The α-Fe_2O_3(0001) surface can expose different terminations consisting of Fe or O ions only. Both iron- and oxygen-terminated surfaces are polar. Despite the intensive studies over the past two decades, the properties of the α-Fe_2O_3(0001) surface are not well understood.[2,3]

Polar oxide surfaces should be unstable[4−6] but are frequently observed. It has been demonstrated[7,8] that polar surfaces can minimize their total energy by forming a long-range periodic structure of domains differing in their work function, which is determined by short-range interactions within the domains. The results of density functional theory (DFT) calculations for the surface structure of various terminations showed that Fe terminations of the α-Fe_2O_3(0001)[9] surfaces are characterized by work function values much lower (by 1.9 eV[9]) than the work function of iron faces (5.07 eV[10]), indicating a significant positive dipole moment, while high work function values of O-terminated surfaces (8.51 eV[9]) imply a large negative dipole moment. Thus, either one of these terminations, whose surface energy is determined by short-range interactions, has a considerable electrostatic energy. This can be reduced by long-range dipole−dipole interactions when the surface is broken up into regions with opposite dipole moments, forming long-range superstructures. These superstructures, called biphase terminations, have been observed by scanning tunneling microscopy (STM) on the α-Fe_2O_3(0001) surfaces. They have been attributed to the coexistence of α-Fe_2O_3(0001) and FeO(111) islands (cf. refs 11−13 and references therein), ferryl (Fe═O) groups coexisting with domains of the Fe-terminated α-Fe_2O_3(0001) surface,[14] or long-range-ordered alternating electropositive and electronegative domains.[15] The surfaces have a common building block[15] consisting of a central oxygen-terminated region surrounded by three Fe and three mixed Fe−O regions in a cyclical arrangement (Figure 1). For a comparison with other STM studies of the nature of these domains, see the Supporting Information.

The superstructure unit meshes on the α-Fe_2O_3(0001) surface,[15] which can be seen in Figure 1, consist of three phases, usually with oxidation state dependent ratios, and denoted as α, β, and γ. The α and γ regions show 5 Å periodicity, while the periodicity of the β region is 3 Å. The α region was tentatively attributed to ferryl termination, the β

Received: July 27, 2021
Revised: November 10, 2021
Published: November 23, 2021

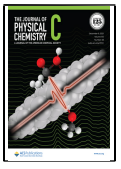

https://doi.org/10.1021/acs.jpcc.1c06656
J. Phys. Chem. C 2021, 125, 26711−26717

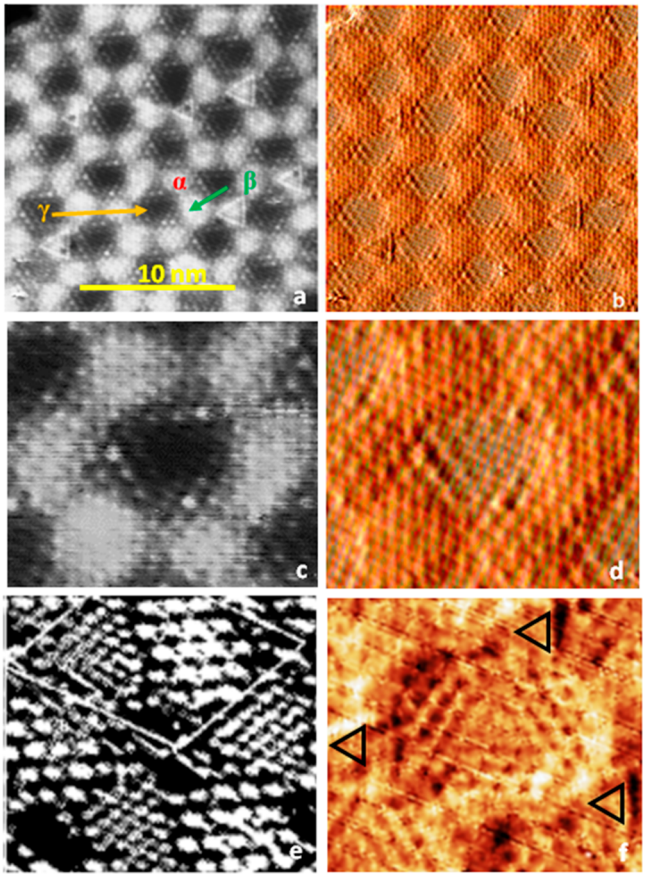

Figure 1. STM images of the hematite biphase surface. (a) Topographic image; (b) current image; (c–f) enlarged views of the building blocks of the biphase, with (c) and (d) from (a) and (b). (e) Constant current image of a hematite single crystal surface; the γ region is not visible under the tunneling conditions used. (f) Surface with a large γ region and triangular islands on the α regions. All images except (e) from thin hematite films.[15] (a–d, f) Adapted from ref 15. Copyright 2016 American Chemical Society. (e) Adapted with permission from ref 12. Copyright 1998 Elsevier.

region was assigned to Fe termination, and the γ region could be assigned clearly to oxygen termination via metal adsorption studies.

The interpretation of STM images is generally not straightforward because the resolved images do not simply reflect a direct topographic map of ion positions on the surface but rather reflect the electronic states that contribute to the tunneling between the tip and the sample.[16] The images of relatively simple surface structures depend on the tunneling current and the applied bias voltage between tip and sample, and they can be calculated with the Tersoff and Hamann (TH) approach.[17,18] This method, based on a perturbative Bardeen theory,[19] provides a physically transparent expression for the tunneling current, which is proportional to the integrated local density of states of the surface in question at the position of the STM tip apex. The TH approach provides a reliable qualitative picture of the surface topography in many standard situations, e.g., in studies of molecular adsorption or surface reconstructions of metal or semiconductor surfaces. However, STM images of nontrivial surface structures can depend critically on the tip–surface separation.[20] In the TH approach the tunneling active wave function of the tip is represented by a spherically symmetric *s*-wave. The *s*-wave approximation of the tip state works well if there is a substantial fraction of electron states with angular momentum $l = 0$ at the tip and if the tip–surface distance is sufficiently large. If there are only few electron s-states at the Fermi energy or the tip–surface distance is too short, then electron states with higher angular momentum contribute to the tunneling and the TH approach is expected to break down. Thus, more complex oxide surfaces, consisting of (partially) positively and negatively charged ions may require treatment within a more sophisticated model including subtler effects of the STM tip. A more sophisticated treatment is needed in particular for Fe oxides in which the density of states near the Fermi level is dominated by d states. An extension of the TH theory, representing the tip electronic structure by higher angular momentum states, has been developed by Chen.[21,22] The latter methodology[19,23] enables treatment of the electronic states of the tip and of the sample separately. As exemplified in Figure S1, at least for some $Fe_2O_3(0001)$ terminations, the TH approach[17,18] and Chen's theory[21,22] give very different STM images. This suggests that more detailed studies using a more sophisticated STM image simulation theory[16,21−23] accounting for the electronic structure of the tip are needed to understand the nature of the termination of the different regions of the iron oxide surfaces.

In this work we present results of extensive simulations of the topography and the superstructures observed in the experimental STM images[15] of various surface terminations of the α-$Fe_2O_3(0001)$ surface. Besides the attempt to explain the experimental observations, the most interesting aspect of all the simulations is the surface termination dependent strong variation with bias and distance, and the tip termination dependence.

METHODOLOGY

DFT-based total energy calculations of the considered surfaces utilized a plane wave basis to represent solutions of the Kohn–Sham equations[24,25] and the projector augmented wave (PAW) method[26] to describe the electron–ion core interactions as implemented in the VASP code. We employed the generalized gradient approximation (GGA) functional, in the PW91[27] and PBE[28] forms with a Hubbard U correction (GGA+U), to treat the strongly correlated Fe 3d electrons[29] and applied an effective parameter U_{eff} of 4.0 eV, respectively.[9] Surface-specific values of U_{eff} for the Fe–Fe–O_3– termination of hematite[30] were also applied. The plane wave basis energy cutoff was set to 500 eV, and the surface Brillouin zone was sampled using a Γ-centered $6 \times 6 \times 1$ k-point mesh with a Gaussian broadening of 0.1 eV. In order to improve the electronic structure description of the surfaces for STM simulations, a denser k-point mesh of $12 \times 12 \times 1$ was applied. The surfaces were modeled by symmetric slabs, and a 1×1 surface unit cell was replicated periodically in space. All systems were structurally optimized with the positions of all atoms fully unconstrained.[9] The details about the slabs used to represent different surface terminations are given elsewhere.[9,15]

The used STM simulation method implemented in the BSKAN code[16,31] is based on Chen's derivative rules[21,22] where the linear combination of tip orbitals is taken into account as corresponding spatial derivatives of the sample single electron wave functions to determine the transmission function of tunneling electrons in the Bardeen current formula.[19] The tip orbitals correspond to the differential operators,[22] which are acting on the single electron wave

https://doi.org/10.1021/acs.jpcc.1c06656
J. Phys. Chem. C 2021, 125, 26711−26717

functions of the sample surface at the tip apex position. The coefficients of the linear combination of the tip orbital states are calculated from the electronic structures of various tip apex atoms (see below) obtained from DFT. This so-called revised Chen's derivative rule method is described in detail elsewhere,[32] and it has proved to simulate STM images in excellent agreement with experiments in several cases considering complex oxides,[33−36] a complex iodide ultrathin film,[37] or complex organic perovskite surfaces,[38] where the Tersoff−Hamann approximation is not always satisfactory. It is worth noting that the mentioned oxides[33,35,36] were on a metal support, whereas for $Fe_3O_4(110)$[34] no metal support was considered. All the DFT calculations for the tip models were performed by using the GGA-PW91 exchange−correlation functional, an energy cutoff of 500 eV for the plane wave basis, and an 11 × 11 × 1 Monkhorst−Pack *k*-point grid to sample the Brillouin zone.

Motivated by the (100) and (111) oriented Pt, Ir, and PtIr tips used in the experiments, we considered in the present STM simulations the following Pt and Ir tips with Pt or Ir atoms at their tops: Pt(001)Pt, Pt(001)Ir, Pt(111)Pt, Pt(111)Ir, Ir(001)Ir, Ir(001)Pt, Ir(111)Ir, and Ir(111)Pt. In most of the cases, initial STM simulations on the iron oxide surfaces did not show significant differences among these eight STM tip models (not shown). Therefore, in this work we focus on pure Pt(001)Pt-based tips with some examples of Pt(111) Pt tips. Here, the atomic model of a pure Pt tip [Pt(001)Pt] corresponds to a five-atom Pt pyramid with a 2 × 2 atom base and an atom adsorbed in its center on top of a Pt(001) substrate five layers thick and 3 × 3 atoms wide, resulting in an asymmetric slab. A Pt lattice constant of 2.775 Å has been used. In selected cases W tip models[39] were also employed.

To compare experiment and theory of STM images of the hematite surfaces, calculations of different terminations were performed. Our previous results for α-$Fe_2O_3(0001)$ surface terminations[9] were used in the present calculations within the same computational setup. STM images for the stable terminations were simulated by using different tips for several tip−surface distances in the range from 3.5 to 5.5 Å, initially for the bias values used in the experiment (−2, +1.4, and +2 V) and later for different biases up to +6 V.

RESULTS AND DISCUSSION

In the [0001] direction the α-Fe_2O_3 surface structure consists of distinctly separate hexagonal Fe and O_3 layers (Figure 2) stacked as a sequence of the bulk repeat unit −Fe−O_3−Fe−. Two (Fe−Fe−O_3− and Fe−O_3−Fe−) of the five basic terminations of the α-$Fe_2O_3(0001)$ surface are Fe-rich, and the remaining three (O_3−Fe−Fe−, O_2−Fe−Fe−, and O−Fe−Fe−) are dominated by oxygen atoms.

In addition, the ferryl (O−Fe−O_3−) termination can be formed by attaching O atoms to the surface Fe atoms of the Fe−O_3−Fe− termination. The labeling of terminations follows the nomenclature of ref 9. The Fe-terminated surfaces have low work functions; the O-terminated surfaces have high work functions. The terminations which were considered in the STM simulations are displayed in Figure 2. The Fe-terminated (stoichiometric) surface is the most stable over a wide range of the oxygen chemical potential μ_O. Only at high μ_O values GGA calculations show that the O_3-terminated surface is energetically preferred,[9] but with GGA+*U* functionals[9,15,30,40] with U_{eff} = 4.0 eV the Fe termination remains stable. However, calculations[41] using a newly developed SCAN meta-GGA

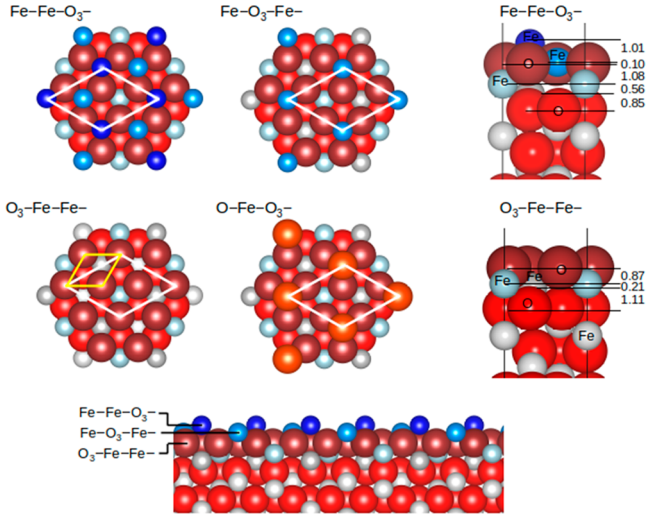

Figure 2. (left and middle) Top and side views of four (Fe−Fe−O_3−, Fe−O_3−Fe−, O_3−Fe−Fe−, and ferryl) bulk terminations of the hematite (α-Fe_2O_3) (0001) surface considered in this work. Fe and O atoms of different layers are represented by small and large balls, respectively. Unit meshes of long and short periodicities are depicted as white and yellow rhombi, respectively. (right) Cross-section image of Fe−Fe−O_3− and O_3−Fe−Fe− terminations showing the relaxed layer distances (in Å).

functional[42] with U_{eff} = 1.8 eV show a preference for an O_3 termination for high μ_O values corresponding to an oxygen-rich limit. This energetic preference results both from an improved description of electron correlations in the semilocal SCAN functional and from a much reduced U_{eff} parameter used in the SCAN+*U* calculation.[41] Thus, the relative energies of the different terminations depend sensitively upon the functional used in the calculations. The energy differences between the considered terminations are small and μ_O dependent, resulting in μ_O-dependent contributions of these terminations to the surface structure.

The connection between simulation and experiment is not straightforward because the tip−sample distance *d* and the state of the tip are not known. Figure 3 displays STM images of the O_3−Fe−Fe− termination of the α-$Fe_2O_3(0001)$ surface simulated by using Pt(111) and Pt(001) tips with a Pt atom apex for different tip−surface distances and biases. For better visualization in all simulated images presented below the contrast was inverted. In the bias range from −2.0 to +2.0 V

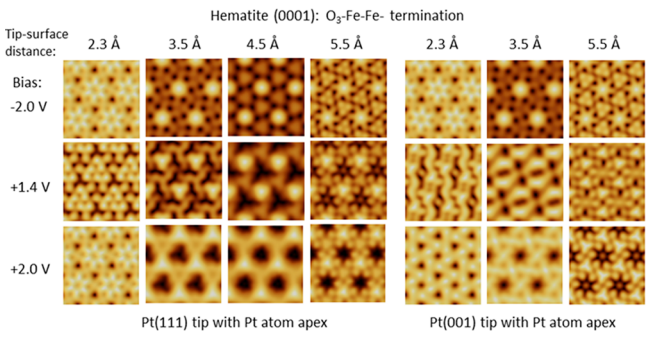

Figure 3. STM images of the O_3−Fe−Fe− termination of the α-$Fe_2O_3(0001)$ surface simulated using Pt(111) and Pt(001) tips with Pt atom apex for different bias values and tip−surface distances. The images are 11.6 Å wide and 11.8 Å high.

https://doi.org/10.1021/acs.jpcc.1c06656
J. Phys. Chem. C 2021, 125, 26711−26717

the calculated images vary strongly with bias, distance, and tip orientation. Variations though weaker are also seen in the images of the Fe−O_3−Fe− termination calculated with the Pt(001)Pt tip as shown in Figure S2. The images for the Pt(111)Pt tip (not shown) are very similar. In contrast to the O_3−Fe−Fe− termination, the Fe−Fe−O_3− termination images are nearly independent of bias, distance, and the state of the tip as illustrated in Figure S2 for −2, +1.4, and +2 V bias values and a Pt(100)Pt tip. No similarity with experiment is obtained for all three surface terminations in this bias range.

In looking for a possible cause of the failure of the STM simulation of the Fe−Fe−O_3− termination, which did not produce the expected short periodicity seen in the experiment, the unrelaxed Fe−Fe−O_3− termination was also considered, based on the following reasoning. The calculations of the various terminations assume that the termination is laterally not confined (because of periodic boundary condition). In reality, however, we have only small patches of three terminations coexisting and the crystal certainly can minimize its surface energy playing the three terminations against each other. DFT calculations actually have shown that the coexistence of small Fe- and O_3-terminated patches has a lower energy per unit area than the combination of large areas of these terminations.[43] STM images of Fe−Fe−O_3− termination of the unrelaxed α-Fe_2O_3(0001) surface are very similar to those for the relaxed case and hardly differ in contrast and applied bias from those displayed in Figure S2 for the Pt(001)Pt tip.

Alternatively, because some of the experimental images were taken with a tungsten tip, in order to check if this can cause the difference between simulation and experiment, the images of the Fe−Fe−O_3− termination of the α-Fe_2O_3(0001) surface were also simulated using a W(111) tip, sharp and blunt W(110) tips, and a 90° rotated W(110) tip with a W atom apex for a tip−surface distance of 5.5 Å and three bias voltages. However, the images (not presented) do not show a clear short periodicity either and also not much difference whether the tip is sharp, blunt, or rotated. In conclusion, none of the Fe−Fe−O_3− images is compatible with experiment in this bias and distance range.

The images for the ferryl (O−Fe−O_3−) termination of the α-Fe_2O_3(0001) surface calculated for a Pt(001)Pt and for a Pt(111)Pt tip (Figure S3) show for all bias voltages the periodicity of the regions assigned tentatively to ferryl in the experimental images (Figure 1). However, the intensity distribution varies considerably with bias, and the best agreement with experiment occurs at negative bias, in disagreement with the other terminations. Agreement must be found for the same bias in all terminations.

Thinking of the possible cause of the failure of the well-established simulation methods to produce the structures derived (in part tentatively) from experiments, we have concluded that it must be the description of the electron transfer (tunneling process) from the tip to the substrate which was not adequately simulated. Hematite is a semiconductor, and its static dielectric constant for bulk oxide as calculated using density functional perturbation theory ranges from 18 to 26.[44] Therefore, tunneling from the tip through the semiconducting oxide substrate has to be adequately simulated.

STM image simulation of semiconductor surfaces requires in general lower bias voltages than those used in experiments due to tip-induced band bending. However, the present calculations showed that the experimental images cannot be explained with a lower bias voltage. This suggests that band bending[45,46] as observed in tunneling into semiconductors (Si, Ge, III−V compounds), which assumes an infinite semiconductor, does not apply to the case of tunneling into a very thin oxide layer on a metal substrate. The fact that no agreement with experiment could be found at biases lower than the bias used in the experiments (simulating band bending) led to the potential model proposed below.

In the tunneling process through a semiconductor layer, a temporary Coulomb blockade may play a role.[47] Tunneling into an unoccupied state on a surface atom on a semiconductor temporarily blocks further current flow until the electron on the atom has diffused to the electrode behind the insulator to which the bias is applied. In order to maintain a continuous current flow therefore, one has to use a higher bias from the very start. Coulomb blockade effects cannot be explicitly included in our present tunneling model. However, in a very simple picture, which may be equivalent to the Coulomb blockade model, the electric field between the tip and the surface atom, which results from the applied voltage between the tip and the substrate (bias), is much too small for tunneling through an insulator/semiconductor. Simulation of tunneling on oxides requires taking the potential drop in the insulator into account. This means that the bias which is needed to obtain correctly simulated STM images is (much) higher than the bias which the experimentalist uses. Therefore, images were calculated for all four terminations using a Pt(001)Pt tip for +2.5 and +3 V and, for still higher bias, from +3 to +6 V. They are displayed in Figures S4−S6. The results of the simulations presented in these figures allow determination of the bias−distance (V, d) combinations, around 3−4.5 V and 3.5−4.5 Å, which give the best agreement with experiment simultaneously for all terminations.

The final selection of the STM images of the four terminations of the α-Fe_2O_3(0001) surface, which provide the best agreements with experiment, simulated for an optimum bias of +3.0 V and tip−surface distance of 4.1 Å, is displayed in Figure 4a−d. The experimental image in the center shows three regions, α, β, and γ, characterized by

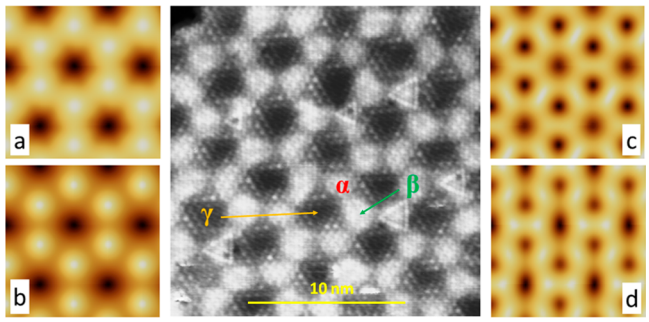

Figure 4. Simulated STM images of the α-Fe_2O_3(0001) surface calculated for an optimum bias of +3.0 V and 4.1 Å tip−surface distance for the terminations (a) O_3−Fe−Fe−, (b) O−Fe−O_3− (ferryl), (c) Fe−Fe−O_3−, and (d) Fe−O_3−Fe−, compared with experimental image. Calculated image width is 11.41 Å and height is 11.20 Å. Experimental STM topography image measured at bias of +2.0 V, current 1.0 nA, and W tip,[15] showing the three regions, α, β, and γ, characterized by different terminations is displayed in the middle panel. Experimental images taken with a Pt-terminated PtIr tip with somewhat lower resolution; e.g., Figure 6 in ref 15 shows the same long-period structure in the α and γ regions while the short-period structure, barely resolved in the W tip image, is not resolved.

https://doi.org/10.1021/acs.jpcc.1c06656
J. Phys. Chem. C 2021, 125, 26711−26717

different terminations. Calculations in finer V, d steps would allow a more precise determination of the optimum V, d combination but were not attempted. It should be emphasized that the STM image contrast is not determined by the topmost layer but by the layer(s) with accessible empty states. An example is the O_3-terminated surface which was identified by Au decoration to be the γ region in Figure 4a.[15] One would expect a 3 Å periodicity but sees the 5 Å periodicity of the Fe layer below it (cf. Figure 2). The long periodicity of the Fe layer may also seem somewhat surprising because the first Fe layer is nearly in the same plane as the second Fe layer and one may suspect that together they give short periodicity, unless the tunneling probability differs strongly between them.

The α domain, which has the same distances and orientation as the γ domain but at a higher level, can be attributed to ferryl termination (Figure 4b). Finally, the short distances and orientation in the β region can be assigned to the Fe−Fe−O_3− or the Fe−O_3−Fe− termination (Figure 4c,d). In these terminations the two Fe layers together form a honeycomb structure, but if a third Fe layer below is involved in the tunneling, the short distance structure seen in the experiment is obtained. An alternative interpretation is the FeO termination, which has been invoked frequently to explain the short distance periodicity in hematite and magnetite. The FeO-like layer on the O_3−Fe−Fe− termination has been simulated in two ways: by adding Fe atoms on top of the O_3−Fe−Fe− termination (i) in "Fe hollows" above the Fe atoms of the subsurface layer and (ii) in "oxygen hollows" over the oxygen atoms of subsurface O_3 layer (Figure S7). For a selected narrow V, d range which gives best agreement with experiment for four terminations simultaneously (Figure 4), the FeO termination calculations show in this V, d range also the short distance pattern expected (Figure S7) so that the FeO termination cannot be excluded.

The terminations obtained from the STM simulations are in good agreement with those expected from energy and work function considerations. The different experimentally labeled regions can be assigned to the calculated most stable terminations. The reported assignment based on the identified STM images in the narrow parameter set found is the following: α, ferryl termination; β, Fe−Fe−O_3− or Fe−O_3−Fe− termination; γ, O_3−Fe−Fe− termination. The energetics of the individual terminations were previously determined[9,15,30,41,48−50] from surface energy (the Gibbs free energy per surface area) plots versus oxygen chemical potential. They show that the energetic rank of the structures proposed for the different regions changes with the oxygen chemical potential μ_O. At intermediate oxygen pressures the Fe−O_3−Fe− surface termination is most stable, at low μ_O the Fe−Fe−O_3− termination is predicted, and at high μ_O the ferryl and O_3−Fe−Fe− termination is predicted by several calculations.

It should be emphasized that previous studies of this system cannot explain the cause or driving force for the formation of the superstructure. Our results suggest that the experimental STM images can be explained by the coexistence of domains of large periodicity, consisting of different low energy hematite terminations. The long-range dipolar interactions caused by the large work function differences between the terminations lead to the formation of the superstructure seen in experiment. There is no doubt that the boundaries between the individual terminations contribute to the energy of the domains. Calculation of this contribution is, however, outside the possibilities of current DFT simulations because of size limitations.

SUMMARY AND CONCLUSION

In this work, great effort is undertaken to simulate the topography of the domains which form long-range superstructures observed in experimental STM images of the hematite (0001) surface. Based on the extensive and detailed calculations of the surface structures of different terminations of the α-Fe_2O_3(0001) surface, the most extensive simulations of the STM images were performed by using the most advanced image simulation procedure implementing Chen's method. It is found that for some surface terminations this method gives images very different from those produced by the method of Tersoff and Hamann. The principal cause of the difference is that, in contrast to Chen's method, the TH approach does not take into account the electronic structure of the tip, which depends not only on tip material but also on tip orientation. Therefore, using an advanced theory of STM image formation such as the one applied in this work is needed for complex oxide systems.

The simulated images allowed making many comparisons of their dependence on tip−surface distance, bias voltage, tip type, orientation, and tip termination. Our results show that the images cannot be explained with the biases used in the experiment but require higher biases. A Pt(100)Pt tip model can reproduce all images at the higher bias, even when a PtIr(100) tip was used in the experiment, probably because a single Pt atom apex is present. The model explanation for the higher bias needed in the calculation is the voltage drop across the dielectric film. Taking this voltage drop into account gives overall agreement with experiment in a narrow range of bias V and distance d. The strong dependence of the images on these parameters suggests that their structure and intensity distribution are dominated by interference effects in the wave field between tip and substrate.[51] This includes the quantum well interferences in the quantum wells between tip and surface and surface and substrate, modulated by the termination-dependent surface structure. Only at the V, d combinations which simulate the experimental conditions can the lateral density of states/height distribution be seen. No information on the normal density of states distribution can be extracted from the image. Thus, starting from the simple density of states/height difference model of STM contrast, the extensive calculations have revealed a much more complex picture of contrast formation.

ASSOCIATED CONTENT

Supporting Information

The Supporting Information is available free of charge at https://pubs.acs.org/doi/10.1021/acs.jpcc.1c06656.

Comparison of different STM studies of the nature of biphase terminations; additional simulated STM images of hematite α-Fe_2O_3(0001) surface terminations for different tips and tip−surface distances (PDF)

AUTHOR INFORMATION

Corresponding Author

Adam Kiejna − *Institute of Experimental Physics, University of Wrocław, 50-204 Wrocław, Poland;* orcid.org/0000-0002-0983-7953; Phone: +48 713759264; Email: adam.kiejna@uwr.edu.pl

https://doi.org/10.1021/acs.jpcc.1c06656
J. Phys. Chem. C 2021, 125, 26711−26717

Authors

Tomasz Ossowski − *Institute of Experimental Physics, University of Wrocław, 50-204 Wrocław, Poland*

Tomasz Pabisiak − *Institute of Experimental Physics, University of Wrocław, 50-204 Wrocław, Poland*

Krisztián Palotás − *Institute for Solid State Physics and Optics, Wigner Research Center for Physics, 1525 Budapest, Hungary; MTA-SZTE Reaction Kinetics and Surface Chemistry Research Group, University of Szeged, 6720 Szeged, Hungary; Department of Theoretical Physics, Budapest University of Technology and Economics, 1111 Budapest, Hungary;* orcid.org/0000-0002-1914-2901

Ernst Bauer − *Department of Physics, Arizona State University, Tempe, Arizona 85287, United States*

Complete contact information is available at: https://pubs.acs.org/10.1021/acs.jpcc.1c06656

Notes

The authors declare no competing financial interest.

■ ACKNOWLEDGMENTS

K.P. acknowledges financial support of the János Bolyai Research Grant of the Hungarian Academy of Sciences (BO/292/21/11), the National Research Development and Innovation (NRDI) Office of Hungary under Project Nos. FK124100 and K131938, and the New National Excellence Program of the Ministry for Innovation and Technology from NRDI Fund (Grant No. ÚNKP-21-5-BME-345).

■ REFERENCES

(1) Cornell, R. M.; Schwertmann, U. *The Iron Oxides: Structure, Properties, Reactions, Occurrences and Uses*, 2nd ed.; Wiley-VCH: Weinheim, Germany, 2003.

(2) Weiss, W.; Ranke, W. Surface Chemistry and Catalysis on Well-Defined Epitaxial Iron-Oxide Layers. *Prog. Surf. Sci.* **2002**, *70*, 1−151.

(3) Parkinson, G. S. Iron Oxide Surfaces. *Surf. Sci. Rep.* **2016**, *71*, 272−365.

(4) Tasker, P. W. The Stability of Ionic Crystal Surfaces. *J. Phys. C: Solid State Phys.* **1979**, *12*, 4977−4984.

(5) Noguera, C. Polar Oxide Surfaces. *J. Phys.: Condens. Matter* **2000**, *12*, R367−R410.

(6) Goniakowski, J.; Finocchi, F.; Noguera, C. Polarity of Oxide Surfaces and Nanostructures. *Rep. Prog. Phys.* **2008**, *71*, 016501.

(7) Vanderbilt, D. Phase Segregation and Work-Function Variations on Metal Surfaces: Spontaneous Formation of Periodic Domain Structures. *Surf. Sci.* **1992**, *268*, L300−L304.

(8) Ng, K.-O.; Vanderbilt, D. Stability of Periodic Domain Structures in a Two- Dimensional Dipolar Model. *Phys. Rev. B: Condens. Matter Mater. Phys.* **1995**, *52*, 2177−2183.

(9) Kiejna, A.; Pabisiak, T. Surface Properties of Clean and Au or Pd Covered Hematite (α-Fe_2O_3) (0001). *J. Phys.: Condens. Matter* **2012**, *24*, 095003.

(10) Derry, G. N.; Kern, M. E.; Worth, E. H. Recommended Values of Clean Metal Surface Work Functions. *J. Vac. Sci. Technol., A* **2015**, *33*, 060801.

(11) Condon, N. G.; Leibsle, F. M.; Lennie, A. R.; Murray, P. W.; Vaughan, D. J.; Thornton, G. Biphase Ordering of Iron Oxide Surfaces. *Phys. Rev. Lett.* **1995**, *75*, 1961−1964.

(12) Condon, N. G.; Leibsle, F. M.; Lennie, A. R.; Murray, P. W.; Vaughan, D. J.; Parker, T. M.; Thornton, G. Scanning Tunneling Microscopy Studies of α-Fe_2O_3(0001). *Surf. Sci.* **1998**, *397*, 278−287.

(13) Lanier, C. H.; Chiaramonti, A. N.; Marks, L. D.; Poeppelmeier, K. R. The Fe_3O_4 Origin of the "Biphase" Reconstruction on α-Fe_2O_3(0001). *Surf. Sci.* **2009**, *603*, 2574−2579.

(14) Lemire, C.; Bertarione, S.; Zecchina, A.; Scarano, D.; Chaka, A.; Shaikhutdinov, S.; Freund, H.-J. Ferryl (Fe = O) Termination of the Hematite α-Fe_2O_3 (0001) Surface. *Phys. Rev. Lett.* **2005**, *94*, 166101.

(15) Lewandowski, M.; Groot, I. M. N.; Qin, Z.-H.; Ossowski, T.; Pabisiak, T.; Kiejna, A.; Pavlovska, A.; Shaikhutdinov, S.; Freund, H.-J.; Bauer, E. Nanoscale Patterns on Polar Oxide Surfaces. *Chem. Mater.* **2016**, *28*, 7433−7443.

(16) Hofer, W. A. Challenges and Errors: Interpreting High Resolution Images in Scanning Tunneling Microscopy. *Prog. Surf. Sci.* **2003**, *71*, 147−183.

(17) Tersoff, J.; Hamann, D. R. Theory and Application for the Scanning Tunneling Microscope. *Phys. Rev. Lett.* **1983**, *50*, 1998−2001.

(18) Tersoff, J.; Hamann, D. R. Theory of the Scanning Tunneling Microscope. *Phys. Rev. B: Condens. Matter Mater. Phys.* **1985**, *31*, 805−813.

(19) Bardeen, J. Tunneling from a Many-Particle Point of View. *Phys. Rev. Lett.* **1961**, *6*, 57−59.

(20) Bode, M.; Pascal, R.; Wiesendanger, R. Distance-Dependent STM-Study of the W(110)/C-R(15 × 3) Surface. *Z. Phys. B: Condens. Matter* **1996**, *101*, 103−107.

(21) Chen, C. J. Origin of Atomic Resolution on Metal Surfaces in Scanning Tunneling Microscopy. *Phys. Rev. Lett.* **1990**, *65*, 448−451.

(22) Chen, C. J. Tunneling Matrix Elements in Three-dimensional Space: The Derivative Rule and The Sum Rule. *Phys. Rev. B: Condens. Matter Mater. Phys.* **1990**, *42*, 8841−8857.

(23) Gottlieb, A. D.; Wesoloski, L. Bardeen's Tunnelling Theory as Applied to Scanning Tunnelling Microscopy: a Technical Guide to the Traditional Interpretation. *Nanotechnology* **2006**, *17*, R57−R65.

(24) Kresse, G.; Hafner, J. Ab initio Molecular Dynamics for Liquid Metals. *Phys. Rev. B: Condens. Matter Mater. Phys.* **1993**, *47*, 558−561.

(25) Kresse, G.; Furthmüller, J. Efficient Iterative Schemes for Ab Initio Total-Energy Calculations Using a Plane-Wave Basis Set. *Phys. Rev. B: Condens. Matter Mater. Phys.* **1996**, *54*, 11169−11186.

(26) Kresse, G.; Joubert, D. From Ultrasoft Pseudopotentials to the Projector Augmented-Wave Method. *Phys. Rev. B: Condens. Matter Mater. Phys.* **1999**, *59*, 1758−1775.

(27) Perdew, J. P.; Chevary, J. A.; Vosko, S. H.; Jackson, K. A.; Pederson, M. R.; Singh, D. J.; Fiolhais, C. Atoms, Molecules, Solids, and Surfaces: Applications of the Generalized Gradient Approximation for Exchange and Correlation. *Phys. Rev. B: Condens. Matter Mater. Phys.* **1992**, *46*, 6671−6687.

(28) Perdew, J. P.; Burke, K.; Ernzerhof, M. Generalized Gradient Approximation Made Simple. *Phys. Rev. Lett.* **1996**, *77*, 3865−3868.

(29) Dudarev, S. L.; Botton, G. A.; Savrasov, S. Y.; Humphreys, C. J.; Sutton, A. P. Electron-Energy-Loss Spectra and the Structural Stability of Nickel Oxide: An LSDA+U Study. *Phys. Rev. B: Condens. Matter Mater. Phys.* **1998**, *57*, 1505−1509.

(30) Huang, X.; Ramadugu, S. K.; Mason, S. E. Surface-Specific DFT + U Approach Applied to α- Fe_2O_3(0001). *J. Phys. Chem. C* **2016**, *120*, 4919−4930.

(31) Palotás, K.; Hofer, W. A. Multiple Scattering in a Vacuum Barrier Obtained from Real-Space Wavefunctions. *J. Phys.: Condens. Matter* **2005**, *17*, 2705−2713.

(32) Mándi, G.; Palotás, K. Chen's Derivative Rule Revisited: Role of Tip-Orbital Interference in STM. *Phys. Rev. B: Condens. Matter Mater. Phys.* **2015**, *91*, 165406.

(33) Lee, T.; Lee, Y.-J.; Palotás, K.; Lee, G.; Stampfl, C.; Soon, A. Polymorphic Expressions of Ultrathin Oxidic Layers of Mo on Au(111). *Nanoscale* **2019**, *11*, 6023−6035.

(34) Walls, B.; Lübben, O.; Palotás, K.; Fleischer, K.; Walshe, K.; Shvets, I. V. Oxygen Vacancy Induced Surface Stabilization: (110) Terminated Magnetite. *Phys. Rev. B: Condens. Matter Mater. Phys.* **2016**, *94*, 165424.

(35) Ly, T. T.; Lee, T.; Kim, S.; Lee, Y. J.; Duvjir, G.; Jang, K.; Palotás, K.; Jeong, S. Y.; Soon, A.; Kim, J. Growing Ultrathin Cu_2O Films on Highly Crystalline Cu(111): A Closer Inspection from Microscopy and Theory. *J. Phys. Chem. C* **2019**, *123*, 12716−12721.

(36) Lee, Y.-J.; Ly, T. T.; Lee, T.; Palotás, K.; Jeong, S. Y.; Kim, J.; Soon, A. Completing the Picture of Initial Oxidation on Copper. *Appl. Surf. Sci.* **2021**, *562*, 150148.
(37) Lee, G.; Lee, Y.-J.; Palotás, K.; Lee, T.; Soon, A. Atomic Structure and Work Function Modulations in Two-Dimensional Ultrathin CuI Films on Cu(111) from First-Principles Calculations. *J. Phys. Chem. C* **2020**, *124*, 16362−16370.
(38) Liu, Y.; Palotás, K.; Yuan, X.; Hou, T.; Lin, H.; Li, Y.; Lee, S.-T. Atomistic Origins of Surface Defects in $CH_3NH_3PbBr_3$ Perovskite and Their Electronic Structures. *ACS Nano* **2017**, *11*, 2060−2065.
(39) Mándi, G.; Teobaldi, G.; Palotás, K. What is the Orientation of the Tip in a Scanning Tunneling Microscope? *Prog. Surf. Sci.* **2015**, *90*, 223−238.
(40) Bandaru, S.; Scivetti, I.; Yam, C.-Y.; Teobaldi, G. The Role of Isotropic and Anisotropic Hubbard Corrections for the Magnetic Ordering and Absolute Band Alignment of Hematite α-Fe_2O_3(0001) Surfaces. *Prog. Nat. Sci.* **2019**, *29*, 349−355.
(41) Si, Y.; Li, M.; Zhou, Z.; Liu, M.; Prezhdo, O. Improved Description of Hematite Surfaces by the SCAN Functional. *J. Chem. Phys.* **2020**, *152*, 024706.
(42) Sun, J.; Ruzsinszky, A.; Perdew, J. P. Strongly Constrained and Appropriately Normed Semilocal Density Functional. *Phys. Rev. Lett.* **2015**, *115*, 036402.
(43) Kiejna, A.; Pabisiak, T. Mixed Termination of Hematite (α-Fe_2O_3) (0001) Surface. *J. Phys. Chem. C* **2013**, *117*, 24339−24344.
(44) Lunt, R. A.; Jackson, A. J.; Walsh, A. Dielectric Response of Fe_2O_3 Crystals and Thin Films. *Chem. Phys. Lett.* **2013**, *586*, 67−69.
(45) Feenstra, R. M. Electrostatic Potential for a Hyperbolic Probe Tip Near a Semiconductor. *J. Vac. Sci. Technol., B: Microelectron. Process. Phenom.* **2003**, *21*, 2080−2088.
(46) Voigtländer, B.; Cherepanov, V.; Korte, S.; Leis, A.; Cuma, D.; Just, S.; Lüpke, F. Invited Review paper: Multi-tip Scanning Tunneling Microscopy: Experimental Techniques and Data Analysis. *Rev. Sci. Instrum.* **2018**, *89*, 101101 (supplementary material).
(47) Guinea, F.; Garca, N. Scanning Tunneling Microscopy, Resonant Tunneling, and Counting Electrons: A Quantum Standard of Current. *Phys. Rev. Lett.* **1990**, *65*, 281−284.
(48) Wang, X. G.; Weiss, W.; Shaikhutdinov, S. K.; Ritter, M.; Petersen, M.; Wagner, F.; Schlögl, R.; Scheffler, M. The Hematite (α-Fe_2O_3) (0001) Surface: Evidence for Domains of Distinct Chemistry. *Phys. Rev. Lett.* **1998**, *81*, 1038−1041.
(49) Bergermayer, W.; Schweiger, H.; Wimmer, E. Ab initio Thermodynamics of Oxide Surfaces: O_2 on Fe_2O_3(0001). *Phys. Rev. B: Condens. Matter Mater. Phys.* **2004**, *69*, 195409.
(50) Rohrbach, A.; Hafner, J.; Kresse, G. Ab initio Study of the (0001) Surfaces of Hematite and Chromia: Influence of Strong Electronic Correlations. *Phys. Rev. B: Condens. Matter Mater. Phys.* **2004**, *70*, 125426.
(51) Schlenhoff, A.; Kovařik, Š.; Krause, S.; Wiesendanger, R. Vacuum Resonance States as Atomic Scale Probes of Noncollinear Surface Magnetism. *Phys. Rev. Lett.* **2019**, *123*, 087202.

https://doi.org/10.1021/acs.jpcc.1c06656
J. Phys. Chem. C 2021, 125, 26711−26717